Proceedings of GT2008
ASME Turbo Expo 2008: Power for Land, Sea and Air
June 9-13, 2008, Berlin, Germany

GT2008-50323

Overspray and Interstage Fog Cooling in Compressor Using Stage-Stacking Scheme – Part 2: Case Study

Ting Wang and Jobaidur R. Khan
Energy Conversion & Conservation Center
University of New Orleans
New Orleans, LA 70148-2220

ABSTRACT

A stage-by-stage wet-compression theory and algorithm have been developed for overspray and interstage fogging in the compressor. This theory and algorithm are used to calculate the performance of an 8-stage compressor under both dry and wet compressions. A 2D compressor airfoil geometry and stage setting at the mean radius are employed. Six different cases with and without overspray have been investigated and compared. The stage pressure ratio enhances during all fogging cases as does the overall pressure ratio, with saturated fogging (no overspray) achieving the highest pressure ratio. Saturated fogging reduces specific compressor work, but increases the total compressor power due to increased mass flow rate. The results of overspray and interstage spray unexpectedly show that both the specific and overall compressor power do not reduce but actually increase. Analysis shows this increased power is contributed by increased pressure ratio and, for interstage overspray, "recompression" contributes to more power consumption. Also it is unexpected to see that air density actually decreases, instead of increases, inside the compressor with overspray. Analysis shows that overspray induces an excessive reduction of temperature that leads to an appreciable reduction of pressure, so the increment of density due to reduced temperature is less than decrement of air density affected by reduced pressure as air follows the polytropic relationship. In contrast, saturated fogging results in increased density as expected.

After the interstage spray, the local blade loading immediately showed a significantly increase. Fogging increases axial velocity, flow coefficient, blade inlet velocity, incidence angle, and tangential component of velocity. The analysis also assesses the use of an average shape factor in the generalized compressor stage performance curve when the compressor stage information and performance map are not available. The result indicates that using a constant shape factor might not be adequate because the compressor performance map may have changed with wet compression. The results of non-stage-stacking simulation are shown to underpredict the compressor power by about 6% and net GT output by about 2% in the studied cases.

NOMENCLATURE

CET	Compressor Exit Temperature (K)
P	Pressure (kPa)
Pc	Compressor Power (kW)
P_{net}	Net GT Output Power (kW)
P_t	Turbine Power (kW)
R	Gas constant (kJ/kg-K)
RH	Relative humidity
r_p	Compressor pressure ratio
SF	Shape factor
T	Temperature (K)
U	Tangential velocity
V	Inlet velocity
V_a	Axial velocity
W	Relative velocity
Wc	Compressor Specific Work (kJ/kg)
W_{Net}	Net Specific Work (kJ/kg)
W_t	Turbine Specific Work (kJ/kg)

Greek

ϕ	Flow coefficient (≡Va/U)
γ	Specific heat ratio
ρ	Density (kg/m^3)
η_C	Overall compressor efficiency (by Eq. 3)
η_p	Polytropic (or small-stage) efficiency
η_{CS}	Overall isentropic compressor efficiency (by Eq. 4)
ψ	Rotor work coefficient ($\equiv \Delta h_0/½U^2$)

Subscripts

1, 2,..	Stage numbers
a	Dry air fraction
c	Compressor
i	Rotor Stage
i+0.5	Stator Stage
t	Turbine

Superscripts

*	Ratio of the off-design value over the design value

INTRODUCTION

When dealing with gas turbine inlet fogging, previous researchers [e.g. 1-3] treated compressor as a single unit and developed the wet compression theory employing only thermodynamic analysis. Under this approach, the interstage fogging cannot be included in the analysis. More complex analyses was then undertaken by researchers [4-11] employing both thermodynamic, heat transfer, and aerodynamic theories through each compressor stage with the help of general performance curves to estimate the compressor aerodynamic performance. Wanting to avoid the uncertainty involved in determining the shape factor when using the general compressor performance curve, a stage-stacking scheme for wet-compression theory has been developed in Part 1 [12] to analyze both inlet overspray and interstage fogging in the compressor. The associated algorithm is integrated into the in-house computational code FogGT [13] to calculate the stage-by-stage compressor performance and the overall gas turbine system performance. In this paper, a case study is

performed on an 8-stage compressor. Six different ambient and overspraying conditions are considered and compared. The analysis also assesses the appropriateness of utilizing an average shape factor in the generalized compressor stage performance curve by back-calculating the shape factor of each stage. Finally, differences between stage-stacking and non-stacking results are compared in this paper.

Studied Cases

The studied compressor has 8 stages. The ISO condition (59°F and 60% Relative Humidity) is used as the design case, and the diameters (hub and tip diameters) are determined at the design condition. The axial velocity (150 m/s) is designed as a constant value throughout the compressor with the following parameters: rotor speed (12,000 RPM), rotor turning angle (12°), inlet pressure (1atm), and isentropic stage efficiency (92%). Note that the axial velocity for non-baseline cases will change due to changed mass flow rate. The wet compression process is represented by a cooling polytropic process with a polytropic index (k) of 1.36. A 2D compressor airfoil geometry and stage setting at the mean radius are employed. The detailed stator and rotor information are given in Table A.3 in the Appendix. All the general assumptions are listed in Part1 and are not repeated here. Six cases are studied with the ISO condition being the baseline; one was studied on a hot day, one was studied on the same hot day with saturated cooling, and the other three cases were studied employing water spray in different locations at the inlet and inside the compressor:

Case 1: Designed baseline case at ISO condition (288K and 60% RH).
Case 2: Under hot weather at 300K and 60% RH
Case 2S: Saturated (0.245%) spray at the 1st rotor inlet at 300K and 60% RH.
Case 3: 2% overspray at the 1st rotor inlet at 300K and 60% RH
Case 4: 2% over spray at stage 1 rotor inlet at 300K and 60% RH and 1% at stage 3 stator inlet
Case 5: 2% spray at stage 1 rotor inlet at 300K and 60% RH and 1% at stage 4 rotor inlet

In this study, the term "fogging" indicates the action of generating the fog. Depending on the amount of the injected water, "saturated fogging" (Case 2S) implies the process of saturating the air to 100% relative humidity and "overspray" implies the process of injecting more than the water amount required to achieve saturated air. Strictly speaking, a 1% overspray implies the amount water that weighs 1% of the dry air flow is injected in addition to the amount required to saturate the air. However, for simplicity, overspay fogging also includes saturated fogging in this study. For example, 2% water overspray with an ambient condition of 300K and 60% RH implies that 0.245% water is needed to saturate the air and (2 – 0.245) = 1.755% is actually used for overspray. In this paper, “dry” air means no water vapor in the air (RH=0); ”moist” air means air contains water vapor but not water droplets (RH>0); and “wet” air means air contains water droplets. The term “dry compression” has been used by industry to indicate compression of dry or moist air with no water droplets. Although it is a misnomer because the air is not completely dry, this paper adopts it nonetheless by following industry practice.

In the Case 1 (design case) simulation, the axial velocity is kept as a constant in each stage by adjusting the flow area (i.e. hub and tip diameters). The variation of hub and tip diameters in different stages is shown in Fig. 1. For the cases of inlet fogging or interstage fogging, the designed geometry is unchanged; the local flow velocity vector, thermal properties, rotor loading condition of each stage are calculated by the stage-stacking scheme. An example showing the effect of fogging on the velocity diagram is illustrated in Fig. 2 by juxtaposing the velocity diagrams of Stage 2 in Cases 1, 2, and 3 for comparison. The following changes are observed:

a. All the velocity directions and magnitude are changed. For example, the absolute rotor inlet velocity changes from purely axial direction to deviating 0.42° for Case 2, –0.26° for Case 2S, and 1.975° for Case 3 from the axis. Interstage spray of Cases 4 and 5 further increases the incidence angles until the water droplets evaporate.
b. The flow coefficient ($\phi = V_a/U$) increases 3% for Case 2, decreases 2.3% for Case 2S, and 24% for Case 3, while the rotor work coefficient Ψ increases 1.5% for Case 2, decreases 3.3% for Case 2S, and decreases 17% for Case 3.

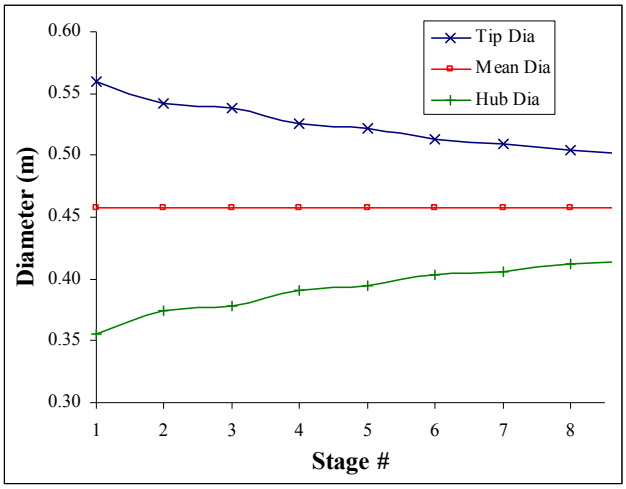

Figure 1 Tip and hub diameters along the compressor

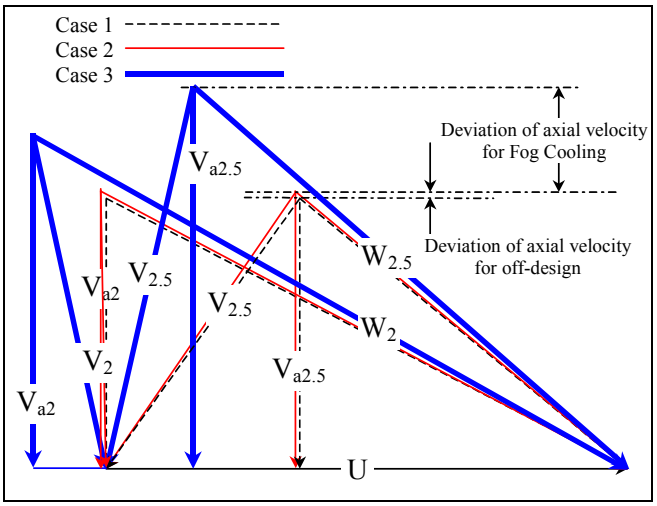

Figure 2 Velocity diagram for Cases 1 and 2 in second stage

RESULTS AND DISCUSSIONS

Static Temperature

Figure 3 shows the static temperature variation in different stages. The temperature for Case 2 is higher than Case 1 in every stage. Saturated fogging (Case 2S) results in temperature reduction in every

stage from Case 2 with a reduction of 6°C, 2°C, and 3°C for the first three stages and 2°C, 3°C, and 4°C for the final three stages, respectively. Overspray (Case 3) significantly reduces the static temperature due to absorption of latent heat during water evaporation. When 2% overspray is applied only at the entrance of the first stage, the temperature drops 6°C, 32°C, and 60°C in the first three stages respectively and maintains an almost constant value for the first three stages before the completion of evaporating all the water droplets.

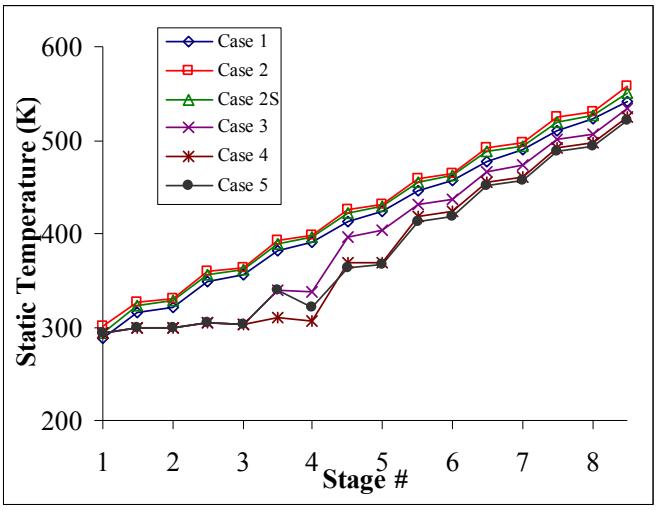

Figure 3 Static temperature variations: overspray induces an excessive reduction of static temperature.

When an additional 1% overspray is applied at the 3rd stage stator (Case 4), the temperature drops further to 30°C below the same stage temperature in Case 3 and 91°C below Case 2. When an 1% overspray is applied at the 4th stage rotor, the temperature drops further to 26°C below the same stage temperature in Case 3 and 76°C below Case 2.

Total Pressure Ratio

Local pressure ratio variations of each stage are shown in Fig. 4. When overspray is applied in the first stage (Case 3), the local pressure ratio experiences a significant drop from 1.4 to 1.1 due to excessive reduction of temperature. This is very different from the condition in saturated fogging case (Case 2S), which the pressure ratio actually increases from 1.4 to 1.44. Not until the third stage when most of the water droplets vaporize, does the local pressure ratio of Case 3 outperforms Cases 1, 2 and 2S. A further spray of water at stage 3 stator in Case 4 keeps the local pressure ratio low at stage 3, but the pressure ratio quickly increases afterwards. Case 5 delays the additional spray to stage 4 rotor and shows a similar trend as in Case 4: the local pressure ratio reduces immediately after spray due to excessive cooling and rises quickly afterwards.

Figure 4 shows interesting local pressure ratio changes in response to local water spray; whereas Fig. 5 shows the overall pressure ratio variations (the integration of the local stage pressure ratio in Fig. 4) for all cases. The pressure ratios of no-fogging Cases 1 and 2 are lowest at 7.45 and 7.23, respectively. Saturated fogging, Case 2S, is shown to achieve the highest overall pressure ratio (8.6), followed by Cases 3, 4, and 5 at 8.42, 8.0 and 7.9, respectively. Increasing pressure ratio due to fogging tends to push the compressor operation towards surge stalling line (not shown here).

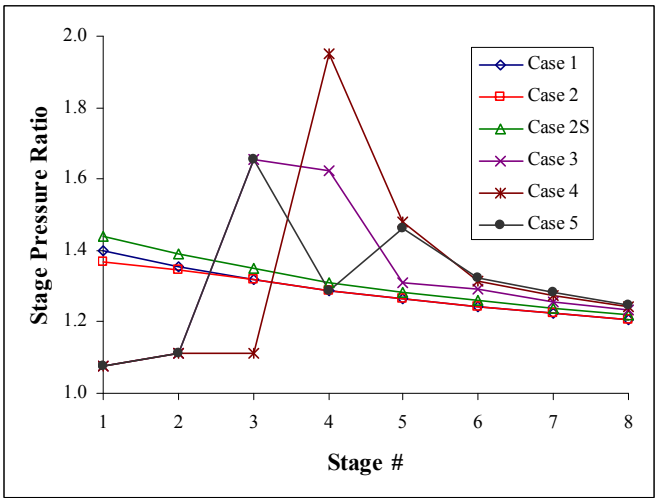

Figure 4 Stage total pressure ratio variation: overspray results in a reduction of local pressure due to an excessive temperature drop, followed by a splurge of pressure rise.

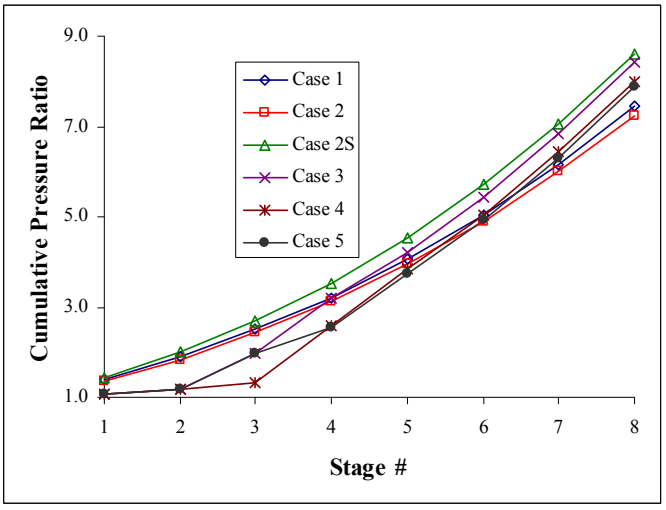

Figure 5 Cumulative compressor total pressure ratio variation

Density

Generally the density increases when fogging is applied due to reduced temperature and the presence of moisture in the air. We are surprised to discover that this general rule only applies to saturated fogging in dry compression; however, it does not apply to the wet compression process with overspray. For example, Fig. 6 shows that the density unexpectedly decreases with the overspray in Cases 3,4, and 5. A further investigation reveals the following reason: When overspray is applied, temperature drops significantly (70 - 90°C) due to water evaporation. This excessive temperature reduction results in a significant reduction in pressure. Pressure usually reduces more than the temperature as it can be seen in the polytropic relation that $PT^{k/(k-1)}$ = Constant, i.e. $P \propto T^{(k-1)/k\gamma}$. Take k = 1.36 for moist air for example, so k/(k-1) = 3.78, which means if the temperature reduces 10%, the pressure will reduce for 33%. Based on the ideal gas law $\rho \sim P/RT$, the density reduces instead of increasing. Although the air receives more water vapor when water droplets vaporize, the slightly increased

density due to water evaporation is not large enough to compensate for the density reduction due to temperature-induced pressure reduction.

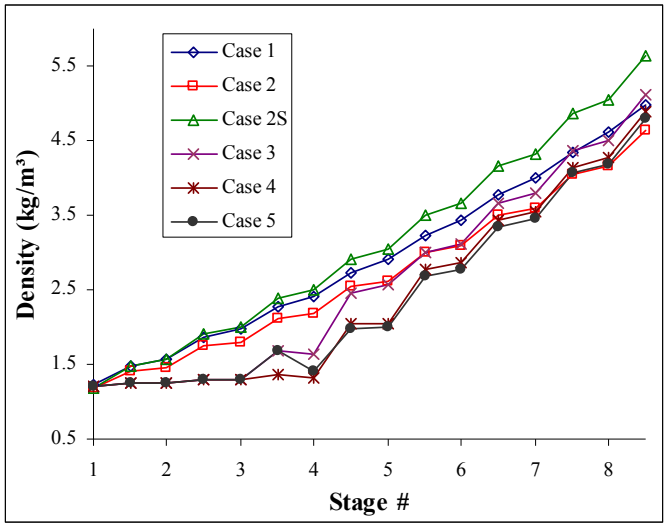

Figure 6 Density variation

Velocity and Flow Coefficient (ϕ)

In the baseline case (Case 1), the axial velocity at each rotor inlet is designed as the same value throughout the compressor. Recall that the algorithm in Part 1 assumes that the compressor performs as a constant-volume flow rate device at the compressor inlet. Once the mass flow rate is established at the inlet, the mass flow is conserved throughout the entire compressor, and the volume flow rate will be adjusted according to the local flow area and density variations. Therefore, all the cases have the same axial velocity at the inlet only. When the ambient temperature rises in Case 2, the density reduces, so the mass flow rate reduces at the inlet. The reduction of density (from Case 1 to Case 2) continues along the compressor results to an increase of axial velocity in Case 2 as shown in Fig. 7. When saturated fogging is applied, the above trend is reversed. The air density increases and mass flow rate increases at the inlet. The increase of density (from Case 1 to Case 2S) continues along the compressor, which results in a decrease of axial velocity as shown in Fig. 7. However, when overspray is applied, excessive cooling produces an appreciable reduction of pressure (Fig. 4), which in turn, results in a reduction in density (see previous explanation in the section of density). Therefore, the air velocity increases. The variation of inlet velocity at each stage is shown in Fig. 7. Significant variations are found in Stages 2 to 5 in Cases 3, 4, and 5, due to the presence of interstage water spray at these stages. Once the water droplets vaporize, the variation trend approaches those of Cases 1 and 2. This velocity change is reflected on the flow coefficient (ϕ) variations in Fig. 8. When overspray is applied at the first stage, the flow coefficient continuously increases up to Stage 3 for Cases 3, 4, and 5 as evaporation has not completed before Stage 3. Once the water completely evaporates, the flow coefficient decreases and approaches Cases 2 and 2S in 6th, 7th, and 8th stages. This trend is coherent with the results obtained by White and Meacock [9]. They showed that the flow coefficient (ϕ) increases till third stage and then decreases and gets lower than the dry compression. Combining the information obtained in Figs. 6 and 8, the result shows that the flow coefficient must significantly increase to accommodate more mass flow rate contributed by overspray especially when the density reduces, rather than increases, after overspray is applied. Whereas, in saturated fogging (Case 2S), no additional mass is added after the compressor inlet and density is persistently higher, so the flow coefficient is low. The striking difference between the saturated fogging and overspray is clearly seen in Fig. 8.

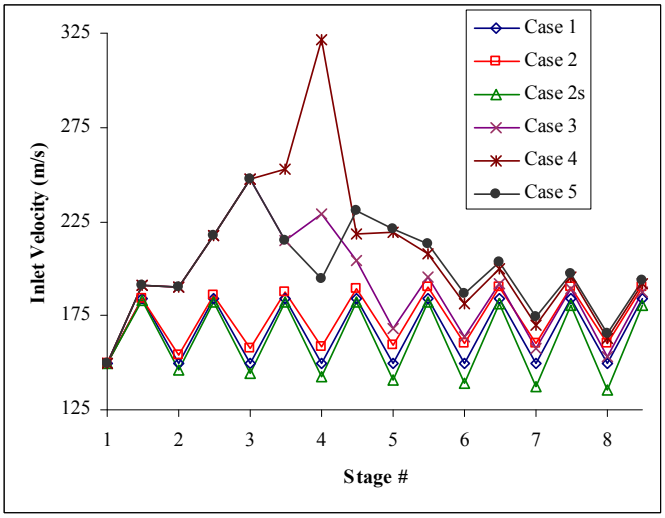

Figure 7 Inlet velocity (actual magnitude) variations at each stage

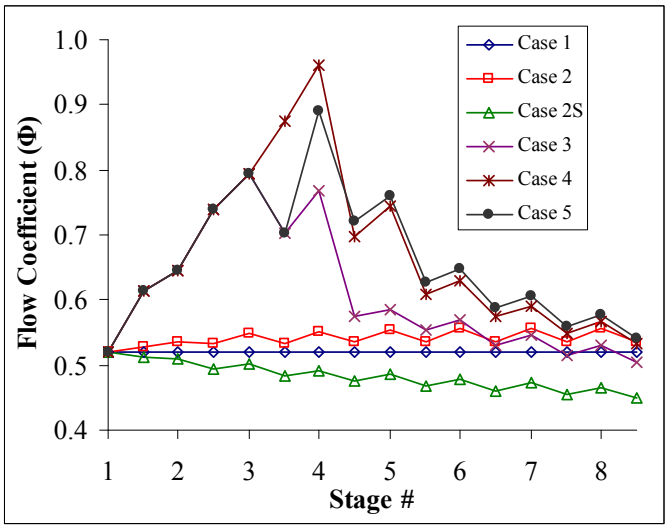

Figure 8 Flow coefficient (ϕ) variations. Note the striking difference between saturated fogging (Case 2S) and overspray (Case 3, 4 and 5).

Work Coefficient (Ψ) and Compressor Power

Changes in compressor power consumption and compressor blade loading are important issues related to fogging. Specific work (kJ/kg) will be discussed separately first via work coefficient (Ψ), followed by stage and integrated power (kW) including the effect of increased mass flow. Figure 9 shows the rotor work coefficient (Ψ), which reflects the specific work normalized by the rotational kinetic energy without including the effect of mass flow rate. This value increases 5-10% when ambient temperature increases 12°C (21.6°F) in Case 2 and

decreases as expected when overspray is applied (Cases 3, 4 and 5). Since the rotor work coefficient is deemed as the specific work of each stage normalized by the rotating kinetic energy, the effect of additional water (vapor) mass is therefore not included. Although the inlet velocity does not change for different cases due to the constant-volume flow rate nature of the compressor, the mass flow rate changes, and therefore, the rotor work co-efficient changes from the very first stage for different cases. It is puzzling to see that overspray reduces the stage work in the early stages, but it significantly increases the work in the later stage. This is in contrast to conventional wisdom that says fogging/overspray can reduce temperature and reduce the compressor's work. This issue will be further investigated and discussed later after the issue of mass flow rate is examined.

When mass flow rate is considered, the required compressor power is shown in Fig. 10. The curve patterns in Fig. 10 are similar to those in Fig. 9, but there are some minor differences. For example, the rotor work coefficient of Case 2 in Fig. 9 is higher than Case 1 because more specific work is required to compress hotter air based on an equal amount of mass flow rate. Whereas, in Fig. 10 the power for Case 2 is almost the same as Case 1 downstream of stage 2 because the hotter air in Case 2 carries less mass flow rate (25.77kg/s for Case 2 vs. 26.91kg/s for Case 1) and requires less compressor power. The reduced mass flow rate self-compensates the reduced compressor efficiency resulting in an almost identical compressor power. Therefore, the effect of mass flow rate is not obvious for Cases 1 and 2 due to this self-compensation effect. Saturated fogging of Case 2S actually brings Case 2 from hot environment to an almost identical condition to ISO case with a mass flow rate of 26.25 kg/s and a power consumption of 7.905 MW, which is the second least among all cases. Similar to its effect on the stage variation of rotor work coefficient (or specific work), overspray reduces the stage power in the earlier stages (1 and 2) but significantly increases the stage power in the later stages. The conventional belief that fogging can reduce the compressor power is violated in the cases of overspray and comes as a surprise. A more thorough investigation is therefore launched and described in detail below.

Figure 11 shows a traditionally textbook-like p-v diagram for an ideal Brayton cycle. If the inlet temperature is cooled from state 1" to 1, the compressor specific work can be qualitatively shown as the area enclosed by the curve and the ordinate axis and is reduced from area 1'-2'-b'-a' to area 1-2-b-a. Indeed many papers have shown fogging/overspray reduces compressor specific work such as the recent papers [4-8] including the paper [3] presented by the authors of this paper. After further investigation, the discrepancy is explained by the following reason: the theoretical GT cycle diagram shown in Fig. 11 is plotted by assuming the pressure ratio maintains at a constant value. In this study, the pressure ratios increase as fogging is applied as shown in Fig. 5. Case 2S gives the highest pressure ratio of 8.6.

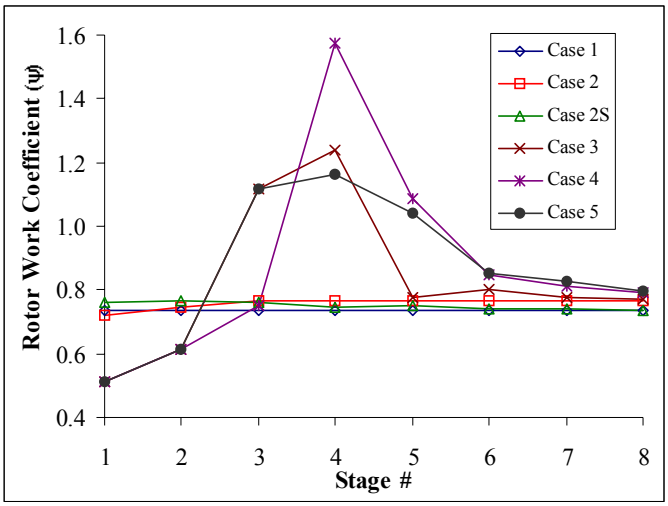

Figure 9 Variation of rotor work coefficient (Ψ).

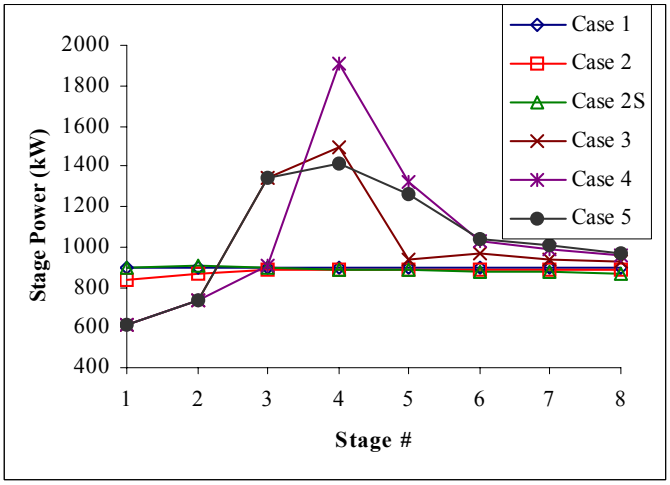

Figure 10(a) Variation of compressor stage power

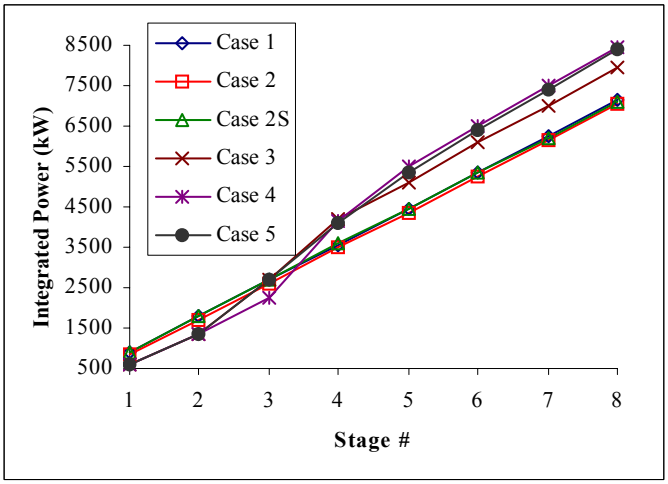

Figure 10(b) Variation of compressor integrated power

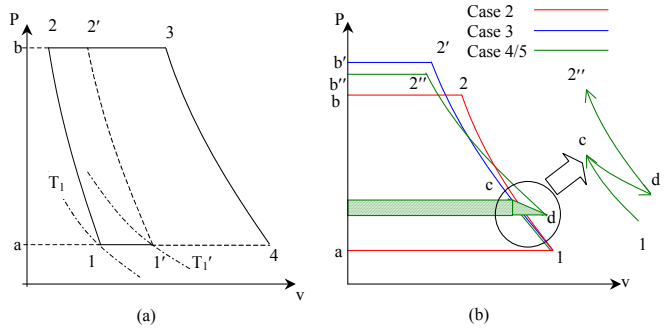

Fig 11: P-v diagrams for the Brayton cycle. (a) Inlet saturated cooling with a constant pressure ratio. (b) Theoretical representation of Cases 2, 3, 4 and 5. The shaded area represents the double compression work due to the interstage spray.

For a clear illustration, Fig. 12 is plotted to show a theoretical representation of the process of Case 3 (1-2" for inlet overspray) and Case 4 (1-c-d-2"' for inlet overspray + interstage spray) on a p-v diagram. It shows that compressor specific work actually increases due to the extra area enclosed by the additional compressor discharge pressure for Cases 2S, 3, 4, and 5. In addition, especially for interstage cooling in Cases 4 and 5, extra work takes place due to the area enclosed by 1-c and d-2". The process c-d shows that the pressure drop is due to additional evaporation. A portion of the shaded area represents the extra power needed for "recompressing" the gas with reduced pressure due to local spray and should be counted twice. If this additional power for pressure increase is more than the savings due to overspray, the total compressor power will increase. This happens for Cases 3, 4, and 5 in this study, but not for Case 2S. The actual process is shown in Figs. 12 and 13. Note that the p-v diagram shows the specific work, which is independent of the mass flow rate, so the added mass due to fogging does not enter into discussion here. The added mass due to water overspray will further exert a negative impact on the compressor's work as shown in Fig. 13. The difference of specific work and power is revealed clearly in Case 2S, where the specific work (249 kJ/kg) is less than that of Case 2 (251 kJ/kg), whereas the power for Case 2S (7.095 MW) is more than that of Case 2 (7.078) due to increased mass flow rate in Case2S.

This additional workload due to overspray also exerts an increased loading requirement to the later stage of the compressor blades as previously shown in Fig. 9. In terms of the velocity diagram, Fig. 7 shows and explains that axial velocity increases, as does the inlet velocity at each stage, which increases the difference between the tangential component of the inlet velocity. The increase of the tangential component of velocity can increase the workload of local stage by 100% (e.g. see Stage 4 in Fig. 7). This significant increase of local blade loading could possibly induce rotating stall and push the overall compressor operation toward the surge limit if the surge limit does not change much from wet compression.

Since both pressure ratio and compressor power increase after overspray fogging is applied, it would be interesting to find out under which conditions, with or without fogging, produce pressure more effectively by comparing the ratio of compressor power/ pressure ratio: P_c/r_p.

The data in Table A2 show the ratio of the compressor power to pressure ratios are 882, 894, 759, 868, 972, and 979 (kW) for Cases 1-5, respectively. Case 2S with the saturated fogging at the GT inlet is most effective among the six cases. Interstage fogging is the least effective.

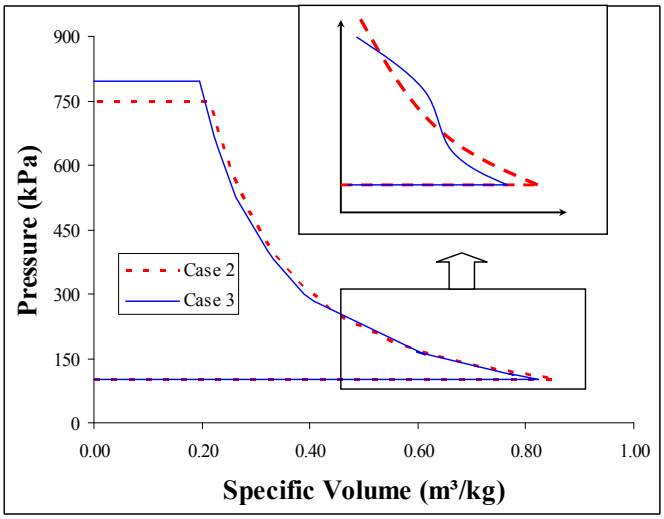

Figure 12 P-v diagram illustration of actual wet compression processes of Cases 2, and 3

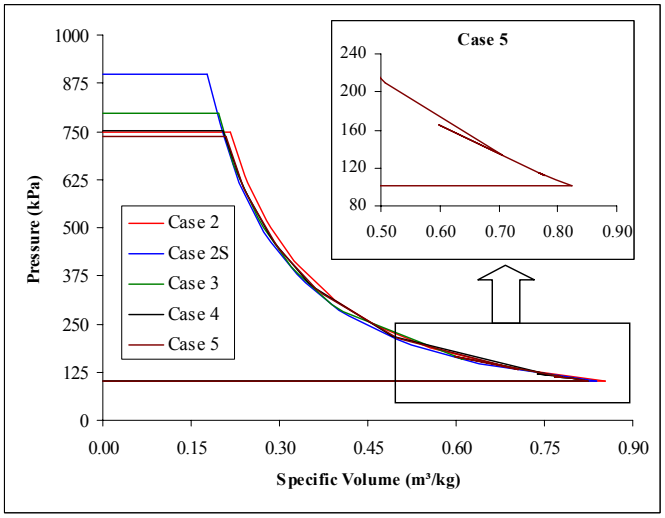

Figure 13 P-v diagram illustration of actual compression processes of Cases 2, 3, and 4. (A portion of the double compression work is qualitatively shown in Fig. 11)

Assessment of Using a Constant Shape Factor and the Generalized Compressor Performance Curve

As stated earlier, one of the objectives of this paper is to assess the use of Shape Factors (SF) by calculating SF from the current results obtained from known compressor geometry and settings. Recall that implementation of the SF approach is a non-voluntary option because the compressor performance maps are deemed proprietary by the manufacturers and generally not available to the public. The concept of SF was introduced by Cerri [14]. The value of SF typically varies between -0.5 and 1. The negative SF values are usually associated with transonic or supersonic stages. Since a detailed stage design for the compressor is not available, an average SF value is usually assigned to all the stages of a compressor. However, SF values are closely dependent on the characteristics of each compressor and vary significantly. Guessing a SF value for a specific engine could

incur a large uncertainty and requires guidance from field test data such as the values shown in [15]. An ill assigned (or guessed) SF value will lead to misleading or even completely false results. Therefore, continuously examining the approach to using SF and providing means to improve it, if possible, are indispensable.

It should be noted that the SF parameter serves as a "tuning" unknown parameter which is determined to minimize the mean square error between measured (or available) data on a gas turbine and the corresponding data computed by the Cycle Program. Only one SF value is determined for each compressor performance map. When calculate the potential changes of pressure ratio, flow coefficient, and work function during wet compression, the same shape factor of dry compression is assumed and is used for each stage such as by Eq. (1) below. This practice implicitly assumes the compressor performance map does not change, and the operating point of each stage during the wet compressor goes on an excursion within the same compressor performance map of the dry compression. This assumption may introduce some errors because Klepper et. al. [16] showed the compressor performance maps changed with wet compression. Since the change of local stage during wet compression has been calculated by using a constant SP in several published papers, we can mathematically back calculate the SP if the operating condition of the local stage is known. To this end, seeing what the SF values are at each stage of this study is interesting. Although back calculating the SF for each stage is not the appropriate way to interpret the function of SF, it is hoped the results of this study will shed some light into the mysterious SF values and provide opportunities for improving the method of utilizing the generalized compressor performance curve.

The procedure for calculating SF value is shown below:

(a) Shape Factor is formulated in equation (1),

$$\psi^* = \psi^*_{max} - \frac{\left(\psi^*_{max}-1\right)\left[\phi^*_{\psi_{max}} + SF\left(\phi^*_{\psi_{max}}-1\right)-\phi^*\right]^2}{\left[\phi^*_{\psi_{max}} + SF\left(\phi^*_{\psi_{max}}-1\right)-1\right]^2} \qquad (1)$$

This is manipulated as a quadratic equation of SF as:

$$a.SF^2 + b.SF + c = 0 \qquad (2)$$

Where, $a = \frac{1-\psi^*}{\psi^*_{max}-1}\left(\phi^*_{\psi_{max}}-1\right)^2$,

$$b = 2\frac{\psi^*_{max}-\psi^*}{\psi^*_{max}-1}\left(\phi^*_{\psi_{max}}-1\right)^2 - 2\left(\phi^*_{\psi_{max}}-1\right)\left(\phi^*_{\psi_{max}}-\phi^*\right),$$

$$c = \frac{\psi^*_{max}-\psi^*}{\psi^*_{max}-1}\left(\phi^*_{\psi_{max}}-1\right)^2 - \left(\phi^*_{\psi_{max}}-\phi^*\right)^2$$

Here, $\psi^* = \frac{\psi}{\psi_D}$ and $\phi^* = \frac{\phi}{\phi_D}$

ψ^*_{max} is the maximum value of all stages

$\phi^*_{\psi_{max}}$ is the ϕ^* value for maximum ψ^*_{max}

According to Muir et. al. [15] the SF values are between 0 and 1. The positive root, which is less than unity found from Eq. (1), is acceptable for this study because the stages are subsonic. Equation (1) is an empirical equation, so the SF value calculated from this equation serves only as a reference value and is subject to further verification. In Eq.(1) the normalized rotor work coefficient has to be greater than unity to find a solution for SF, otherwise Eq. (1) no longer holds true. This is based on the design practice that the design point is optimized and the off-design condition will require more compressor work. The condition of normalized rotor work coefficient being greater than unity has made Eq. (1) not applicable when inlet or interstage fogging is used, especially when the rotor work coefficient increases.

The result shows the stage SF value varies between 0.55 and zero for Case 2S, between 0.95 and zero for Case 2 and between 0.6 and -0.05 for fogging Case 3 (See Table A2 in Appendix). The negative SF value at stage 4 in Case 3 implies the air velocity is very high. The large variation of SF values from stage to stage and from case to case implies the conventional practice of selecting a single SF value to represent one specific compressor, especially fogging/overspray, may not be appropriate and requires improvement. Some of the values of SF are out of range in Table A2. The approach of assigning a single SF value in employing the generalized compressor performance curve will be a subject for future study.

Overall GT System Analysis

The unexpected result of both increased compressor specific power and total power due to fogging raised our anxiety concerning finding out its impact on the overall gas turbine output and efficiency. To this end, the pressure ratio obtained from the stage-stacking result is used as input to the FogGT program [3 or 13]. In addition, the overall compressor efficiency is calculated from Eq. 3 (same as Eq. 10 of Part 1 [12]) and provided as an input to FogGT.

$$\eta_C \approx \frac{r_P^{(k-1)/k}-1}{r_P^{(k-1)/k\eta_P}-1} \qquad (3)$$

In the meantime, the overall compressor efficiency obtained by Eq. 3 is also compared with the isentropic compressor efficiency defined in Eq. 4 as the ratio of isentropic compressor power (Pc_s) and actual compressor power (P_c) from stage-stacking result.

$$\eta_{CS} = \frac{Pc_s}{Pc} \qquad (4)$$

Since FogGT treats the compressor as a blackbox, the interstage fogging of Cases 4 and 5 cannot be adequately simulated before the stage-stacking scheme is fully incorporated into FogGT. Hence, only Case 3 is submitted for GT system simulation. The overall GT system performance and comparison between stage-stacking and non-stacking schemes are shown in Table 1.

First, let us examine the difference between the stage-stacking and FogGT (non-stacking) results of the overall compressor power. For Cases 1 and 2, the differences are small, at about 2.2% and 0.74%, respectively. For overspray case (3), FogGT underpredicts the compressor power by about 6%. These differences are caused by minor differences of moist air specific heat, which is kept as a constant value of 1.38 during stage-stacking calculation as well as in Eq 3. Nonetheless, FogGT, similar to the stage-stacking scheme, also calculates higher compressor power (P_c) and specific work (W_c) for Case 3 than non-fogging cases (1 and 2). Although ovespray requires more compressor power, it also produces higher pressure ratio. Therefore, to fairly evaluate the compressor performance, comparison of the power consumed by raising per unit pressure ratio is made. In Table 1, Case 3 shows improved compressor effectiveness by about 3% from Case 2 (0.97MW vs. 0.94MW per unit pressure ratio).

Table 1 Comparison of stage-stacking and non-stacking results for compressor and the GT system.

Cases		Case 1	Case 2	Case 2S	Case 3
CET (K)	Non-stacking	540.2	562.8	581.4	520.4
	Stacking	**541.9**	**557.9**	**551.1**	**533.4**
Specific Works	Wc (kJ/kg) [Non-stacking]	259.4	274.7	301.9	286.3
	Wc (kJ/kg) [Stacking]	**265.3**	**272.6**	**270.2**	**297.6**
	W_f (kJ/kg) [Non-stacking]	11.39	11.52	12.57	13.72
	W_t (kJ/kg) [Non-stacking]	592.2	592.1	633.7	648.5
	W_{net} (kJ/kg) [Non-stacking]	321.4	305.9	319.3	348.4
P_c (kW)	Non-stacking	6981	7078	7905	7497
	Stacking	**7139**	**7026**	**7093**	**7948**
	% of difference	**2.26%**	**-0.74%**	**-10.3%**	**6.01%**
P_f (kJ/kg) [non-stacking]		306.5	296.9	329.2	359.4
P_t (kJ/kg) [non-stacking]		15935	15259	16594	16981
P_{net} (kW)	Non-Stacking	8648	7883	8360	9124
	Stacking	**8490**	**7936**	**9172**	**8674**
	% of difference	**-1.83%**	**0.67%**	**9.71%**	**-4.94%**
Air flow rate (kg/s)		26.91	25.77	26.19	26.19
Inlet Air Density (kg/m^3)		1.222	1.170	1.193	1.213
Fuel flow rate (kg/s)		0.5787	0.5484	0.5484	0.6059
Thermal Efficiency [Non-stacking]		29.86%	28.73%	30.46%	30.09%
Overall Compressor Efficiency (%)	**From Pc_s/Pc**	**87.53**	**90.22**	**99.78**	**84.48**
	From Eq. 3	**89.51**	**89.55**	**89.53**	**89.56**
	% of difference	**2.26%**	**-0.74%**	**-10.3%**	**6.01%**
Pressure Ratio [Stacking]		**7.45**	**7.23**	**8.59**	**8.42**
Power/Pressure Ratio (kW) [Stacking]		958.4	971.9	825.4	943.8

(Net output power = Turbine power -fuel pump power -compressor power)

In Table 1, the compressor efficiency defined by Eq. (3) shows the compressor efficiency is not affected by overspray (89.55% vs. 89.56%). However, the isentropic efficiency defined by Eq. (4) shows a significant decrease from 90.22% to 84.54% due to fogging. It seems puzzling why fogging results in such a big reduction of isentropic efficiency. A further investigation discovered that the referenced isentropic power for each case is different because the inlet temperature is different. The overspray case (Case 3) is based on a lower isentropic power than nonfogging case (Case 2). Hence, the isentropic efficiency reduces. Therefore, the most fair way for comparing the compressor effectiveness still goes back to the last row in Table 1, as Pc/p_r.

Regarding the turbine output, both the specific turbine output work (W_t) and the total turbine power (P_t) increase, resulting in a significant net GT output power increase of 15.7% for Case 3. Most people attribute the increased net GT output power to the increased mass flow rate for overspray cases. Actually, most of the credit should be given to the specific network output increase, which already contributes up to 14.1%. If the specific net output work were not increased much, we then could conclude that the increased net output is attributed to increased mass flow rate. Increased mass flow rate is not the major cause of increased GT output power because increased mass flow rate also contributes to increased consumption of compressor power. Despite the significant increase of GT net output power, the efficiency only increases 1.2 percentage points (or 4.7%). If the compressor power calculated by stage-stacking scheme is used for output power and efficiency calculation, the output enhancement will be 9.35%, and the thermal efficiency will be almost the same.

Comparison with previous studies in compressor power consumption and compressor efficiency for wet compression

The present result of reduced isentropic compressor efficiency due to wet compression is consistent with Sanaye et. al. [17] Abdelwahab [18], and Roumeliotis and Mathioudakis [19], but inconsistent with Bagnoli et. al. [6]. The present result of increased compressor power consumption due to wet compression is consistent with Bagnoli et. al. [6] and Roumeliotis and Mathioudakis [19], but inconsistent with Sanaye et. al. [17] Abdelwahab [18]. The present result of increased **specific** compressor power due to wet compression, to the authors' knowledge, has not been presented by other researchers in the open literature. A recap of previous studies are summarized below:

Bagnoli et. al. [6] used the Shape Factor for the calculation, but they did not mention the criteria for its selection. The shape factor determined the stage efficiency and constant shape factor were used for all stages. Their results showed that compressor power increased with an increase of injected water and efficiency also increased with an increase of injected water. Sanaye et. al. [17] also used constant shape factor value to calculate each stage performance and showed that the pressure ratio increases with an increase of injected water amount. Their results showed that both the compressor efficiency and compressor power decrease with an increase of injected water amount. Abdelwahab [18] showed a shift in peak efficiency to higher flow rates as well as deterioration in the peak efficiency as the water injection rates increase. His results showed that stage speed increased due to water injection to achieve higher design pressure ratio. Both the power reduction capability and the polytropic efficiency decrease with the increase of the stage pressure ratio.

It is encouraging to know that the present results are supported by the recent experimental results from Roumeliotis and Mathioudakis [19]. They showed that the compressor power increased by water injection and the increased compressor power was linear with the quantity of water entering the stage. As a result, the compressor isentropic efficiency decreases linearly with the amount of water injected.

SUMMARY

Employing the wet compression theory and the stage-stacking scheme, six fogging and non-fogging cases have been investigated and compared. The results show:

(a) The compressor performance of saturated fogging (dry compression) is strikingly differently from overspray (wet compression). The stage pressure ratio enhances during all fogging cases as does the overall pressure ratio. With saturated fogging (no overspray), the compressor achieves the highest pressure ratio and requires less specific compressor work than without fogging. However, the results of overspray and interstage spray unexpectedly show that both the specific and overall compressor power do not reduce but actually increase. Analysis shows this increased power is contributed by increased pressure ratio, and for interstage overspray, "recompression" contributes to more power consumption.

(b) Saturated fogging (Case 2S) brings down the specific compressor work from a hot ambient condition (Case 2); however, due to increased mass flow, the overall compressor power increases.

(c) It is unexpected to see that air density actually decreases, instead of increases inside the compressor with overspray. Analysis shows that overspray induces an excessive reduction of temperature which leads to an excessive reduction of pressure, so the increment of density due to reduced temperature is less than decrement of air density affected by reduced pressure as air follows the polytropic relationship. In contrast, saturated fogging results in increased density as expected.

(d) The compressor power/ pressure ratio values show that saturated fogging is most effective in producing pressure ratio, whereas interstage fogging is least effective.

(e) The local blade loading significantly increases immediately after the interstage spray. In this study, a 2% interstage fogging can

increase the local blade loading up to 100%. This significant increase of local blade loading could induce rotating stall locally near the spray location.

(f) Overspray increases axial velocity, flow coefficient, the blade inlet velocity, the incidence angle, and the tangential component of velocity. Saturated fogging results in opposite phenomena.

(g) Shape factor used in the generalized compressor performance curve varies throughout the compressor stages in the present study. Therefore, using one single shape factor value throughout the compressor may not be adequate, nor is it appropriate to use the same shape factor value for both dry and wet compression.

(h) Using the pressure ratio obtained from stage-stacking scheme to calculate the overall GT performance shown non-stage-stacking system simulation could underpredict the compressor power by about 6% and net GT output by about 2% in 1% oversprayed case.

ACKNOWLEDGEMENT

This study was supported by the Louisiana Governor's Energy Initiative via the Clean Power and Energy Research Consortium (CPERC) and administered by the Louisiana Board of Regents.

REFERENCES

1. Zheng, Q., Sun, Y., Li, S. and Wang, Y, 2002, "Thermodynamic Analysis of Wet Compression Process in the Compressor of Gas Turbine", Proc. of ASME Turbo Expo 2002, Amsterdam, The Netherlands, June 3-6, ASME Paper No: GT-2002-30590.
2. Zheng, Q., Li, M., Sun, Y., 2003, "Thermodynamic Analysis of Wet Compression and Regenerative (WCR) Gas Turbine", Proceedings of ASME Turbo Expo 2003, Atlanta, Georgia, USA, June 16-19, ASME Paper No: GT-2003-38517.
3. Khan, J. R. and Wang, T., 2006, "Fog and Overspray Cooling for Gas Turbine Systems with Low Calorific Value Fuels", Proceedings of ASME Turbo Expo 2006, Barcelona, Spain, May 8-11, 2006, ASME Paper No: GT-2006-90396.
4. Li, M. and Zheng, Q., 2004, "Wet Compression System Stability Analysis", Proceedings of ASME Turbo Expo 2004, Vienna, Austria, June 14-17, 2004, ASME Paper No: GT-2004-54018.
5. Payne, R.C. and White, A.J., 2007, "Three-Dimensional Calculations of Evaporative Flow in Compressor Blade Rows", Proceedings of ASME Turbo Expo 2007, Montreal, Canada, May 14-17, 2007, ASME Paper No: GT-2007-27331.
6. Bagnoli, M., Bianchi, M., Melino, F. and Spina, P.R., 2006, "Development and Validation of a Computational Code for Wet Compression Simulation of Gas Turbines", Proceedings of ASME Turbo Expo 2006, Barcelona, Spain, May 8-11, 2006, ASME Paper No: GT-2006-90342.
7. Bagnoli, M., Bianchi, M., Melino, F., Peretto, A., Spina, P.R., Ingistov S. and Bhargava, R.K., 2006, "Application of a Computational Code to Simulate Interstage Injection Effects on GE Frame 7EA Gas Turbine", Proceedings of ASME Turbo Expo 2006, Barcelona, Spain, May 8-11, 2006, ASME Paper No: GT-2006-90343.
8. Bianchi, M., Melino, F., Peretto, A., Spina, P.R. and Ingistov S., 2007, "Influence of Water Droplet Size and Temperature on Wet Compression", Proceedings of ASME Turbo Expo 2007, Montreal, Canada, May 14-17, 2007, ASME Paper No: GT-2007-27458.
9. White A J.., Meacock A J., 2004, "An evaluation of the effects of water injection on compressor performance", ASME J. of Engineering for Gas Turbines and Power, Vol. 126, pp.748-754.
10. Meacock A. J., White A. J., 2006 "The Effect of Water Injection on Multi – Spool Gas Turbine Behaviour", ASME J. of Engineering for Gas Turbines and Power, Vol. 128, pp 97-102, also ASME paper GT2004-53320.
11. Roumeliotis I., Mathioudakis K., 2006, "Evaluation of Interstage Water Injection Effect on Compressor and Engine Performance", ASME Journal of Engineering for Gas Turbine and Power, Paper GTP-05-1123, Vol. 128/4, pp. 849-856, also ASME paper 2005-GT-68698.
12. Wang, T. and Khan, J.R., 2008, "Overspray and Interstage Fog Cooling in Compressor using Stage-Stacking Scheme—Part 1: Development of Theory and Algorithm" manuscript submitted to ASME Turbo Expo2008, Berlin, Germany, June 9-13, 2008, ASME Paper No: GT-2008-50322.
13. Khan, J. R. and Wang,T., "Development of the Computational Program FogGT for Wet Compression via Fog/Overspray Gas Turbine Inlet Cooling," ECCC Report 2005-07, Energy Conversion and Conservation Center, University of New Orleans, October 2005.
14. Cerri et al. (1993) (Cerri, G., Salvini, C., Procacci, R., Rispoli, F., 1993, "Fouling and Air Bleed Extracted Flow Influence on Compressor Performance", ASME Paper 93-GT-366)
15. Muir, D. E., Saravanamuttoo, H. I. H. and Marshall, D. J., 1989, "Health Monitoring of variable Geometry Gas Turbine for the Canadian Navy", ASME Journal of Engineering for Gas Turbines and Power, Vol. 124, pp. 155-160.
16. Klepper J., Hale A., Davis M., Hurwitz W., "A Numerical Investigation of the Effects of Steam Ingestion on Compression System Performance", ASME paepr No. GT2004-54190.
17. Sanaye, S., Rezazadeh, H., and Aghazeynali, M., 2006, "Effects of Inlet Fogging and Wet Compression on Gas Turbine Performance", Proceedings of ASME Turbo Expo 2006, Barcelona, Spain, May 8-11, 2006, ASME Paper No: GT-2006-90719.
18. Abdelwahab, A., 2006, "An Investigation Of The Use Of Wet Compression In Industrial Centrifugal Compressors", Proceedings of ASME Turbo Expo 2006, Barcelona, Spain, May 8-11, 2006, ASME Paper No: GT-2006-90695.
19. Roumeliotis, I and Mathioudakis, K., 2007, "Water Injection Effects on Compressor Stage Operation", ASME Journal of Engineering for Gas Turbines and Power, Vol. 129, pp. 778-784.

APPENDIX

Table A1 Detailed stage-stacking data (pressures, temperature, velocity, flow coefficient, Mach numbers and density) for all cases. (Shaded areas represent the stator in corresponding stage and the non-shaded rows represent rotor stages.)

Stage	Total Pressure (kpa)					
	Case 1	Case 2	Case 2S	Case 3	Case 4	Case 5
1	115.6	115.1	116.1	106.1	106.1	106.1
1.5	161.6	157.4	167.0	114.3	114.3	114.3
2	161.6	157.4	167.0	114.3	114.3	114.3
2.5	219.0	211.7	232.5	127.1	127.1	127.1
3	219.0	211.7	232.5	127.1	127.1	127.1
3.5	288.6	279.4	313.8	210.3	141.4	210.3
4	288.6	279.4	313.8	210.3	141.4	210.3
4.5	371.8	359.6	410.7	341.0	275.7	270.6
5	371.8	359.6	410.7	341.0	275.7	270.6
5.5	469.5	454.0	526.4	445.9	407.9	395.0
6	469.5	454.0	526.4	445.9	407.9	395.0
6.5	583.0	563.8	662.0	575.7	535.9	521.6
7	583.0	563.8	662.0	575.7	535.9	521.6
7.5	713.0	689.5	819.0	723.9	683.2	669.0
8	713.0	689.5	819.0	723.9	683.2	669.0
8.5	861.2	831.7	997.8	893.7	850.2	835.1

Stage	Static Pressure (kpa)					
	Case 1	Case 2	Case 2S	Case 3	Case 4	Case 5
1	101.3	101.3	101.3	101.3	101.3	101.3
1.5	134.9	132.2	138.2	107.2	107.2	107.2
2	144.9	139.3	148.1	107.3	107.3	107.3
2.5	185.9	180.1	196.4	114.4	114.4	114.4
3	202.3	188.6	209.2	112.0	112.0	112.0
3.5	248.5	240.4	268.9	165.2	121.3	165.2
4	271.9	251.2	285.8	159.7	115.0	132.7
4.5	324.1	312.8	356.8	282.8	219.2	209.2
5	355.0	325.7	377.8	300.7	218.8	213.5
5.5	413.6	398.7	462.4	381.2	340.7	326.0
6	452.8	414.2	488.6	399.8	356.0	341.3
6.5	518.2	499.5	587.0	500.8	459.9	445.0
7	566.2	517.8	618.4	524.4	480.2	464.3
7.5	639.0	615.4	732.4	638.2	597.0	582.4
8	696.2	636.4	769.2	667.2	622.3	606.8
8.5	777.3	748.2	899.8	796.9	752.8	737.6

Stage	Static Temperature (K)					
	Case 1	Case 2	Case 2S	Case 3	Case 4	Case 5
1	288.0	300.0	294.2	294.2	294.2	294.2
1.5	315.2	326.3	322.1	299.1	299.1	299.1
2	321.7	331.2	328.0	299.2	299.2	299.2
2.5	348.0	359.0	356.2	305.1	305.1	305.1
3	356.5	363.8	362.2	303.3	303.3	303.3
3.5	380.7	392.6	389.7	340.1	310.6	340.1
4	390.6	397.5	396.1	337.1	306.2	321.0
4.5	413.3	425.9	422.7	396.5	368.9	364.2
5	424.2	430.9	429.1	403.0	368.7	366.1
5.5	445.7	459.1	455.3	431.8	418.3	413.1
6	457.4	464.2	462.0	437.3	423.2	418.2
6.5	478.0	492.3	487.5	466.9	455.7	451.5
7	490.2	497.4	494.3	472.6	461.0	456.6
7.5	510.0	525.2	519.5	500.5	491.1	487.6
8	522.6	530.3	526.3	506.4	496.5	493.0
8.5	541.9	557.9	551.1	533.4	524.8	521.7

Stage	Density (kg/m³)					
	Case 1	Case 2	Case 2S	Case 3	Case 4	Case 5
1	1.2225	1.1705	1.1926	1.2131	1.2131	1.2131
1.5	1.4879	1.4049	1.4861	1.2550	1.2550	1.2550
2	1.5656	1.4583	1.5636	1.2556	1.2556	1.2556
2.5	1.8561	1.7391	1.9095	1.3017	1.3017	1.3017
3	1.9717	1.7973	2.0005	1.2845	1.2845	1.2845
3.5	2.2688	2.1226	2.3891	1.6709	1.3537	1.6709
4	2.4190	2.1901	2.4989	1.6302	1.3127	1.4177
4.5	2.7213	2.5386	2.9116	2.4538	2.0376	1.9699
5	2.9038	2.6123	3.0362	2.5674	2.0349	1.9991
5.5	3.2194	2.9983	3.5041	3.0111	2.7650	2.6811
6	3.4347	3.0814	3.6514	3.1179	2.8541	2.7705
6.5	3.7637	3.5076	4.1576	3.6698	3.4260	3.3437
7	4.0091	3.5985	4.3191	3.7953	3.5408	3.4531
7.5	4.3488	4.0499	4.8658	4.3585	4.1370	4.0636
8	4.6231	4.1479	5.0458	4.5021	4.2626	4.1882
8.5	4.9789	4.6346	5.6368	5.1114	4.8766	4.8047

Stage	Inlet Velocity (m/s)					
	Case 1	Case 2	Case 2S	Case 3	Case 4	Case 5
1	150.00	150.00	150.00	150.00	150.00	150.00
1.5	183.68	183.96	183.40	191.34	191.34	191.34
2	150.00	154.23	146.57	190.27	190.27	190.27
2.5	183.68	185.67	182.16	217.59	217.59	217.59
3	150.00	157.61	144.48	247.47	247.47	247.47
3.5	183.68	187.67	182.35	215.12	252.75	215.12
4	150.00	158.63	142.27	229.00	321.80	194.93
4.5	183.68	188.98	182.14	204.15	218.45	230.30
5	150.00	159.65	140.79	168.40	219.29	221.44
5.5	183.68	189.86	181.93	195.90	207.63	213.01
6	150.00	160.10	138.75	164.02	181.08	186.62
6.5	183.68	190.30	181.34	192.28	200.17	203.25
7	150.00	160.03	137.14	157.38	170.22	174.57
7.5	183.68	190.47	180.83	189.59	195.19	197.21
8	150.00	160.09	135.57	153.10	163.06	165.94
8.5	183.68	190.53	180.27	187.66	192.08	193.45

Stage	Absolute Mach Number					
	Case 1	Case 2	Case 2S	Case 3	Case 4	Case 5
1	0.440	0.431	0.435	0.439	0.439	0.439
1.5	0.515	0.507	0.508	0.553	0.553	0.553
2	0.417	0.422	0.402	0.550	0.550	0.550
2.5	0.491	0.488	0.480	0.620	0.620	0.620
3	0.396	0.411	0.378	0.708	0.708	0.708
3.5	0.469	0.471	0.459	0.578	0.714	0.578
4	0.378	0.396	0.356	0.618	0.919	0.538
4.5	0.450	0.455	0.440	0.508	0.563	0.597
5	0.363	0.382	0.337	0.416	0.565	0.573
5.5	0.433	0.440	0.423	0.465	0.500	0.516
6	0.349	0.369	0.321	0.387	0.433	0.449
6.5	0.418	0.426	0.408	0.440	0.462	0.471
7	0.337	0.357	0.306	0.358	0.391	0.402
7.5	0.405	0.413	0.394	0.419	0.434	0.440
8	0.327	0.345	0.293	0.336	0.361	0.368
8.5	0.393	0.401	0.381	0.402	0.413	0.417

Stage	Relative Mach Number					
	Case 1	Case 2	Case 2S	Case 3	Case 4	Case 5
1	0.953	0.932	0.932	0.949	0.949	0.949
1.5	0.661	0.659	0.659	0.802	0.802	0.802
2	0.902	0.900	0.900	1.090	1.090	1.090
2.5	0.629	0.627	0.627	0.913	0.913	0.913
3	0.856	0.862	0.862	1.258	1.258	1.258
3.5	0.602	0.594	0.594	0.792	1.036	0.792
4	0.818	0.821	0.821	1.109	1.457	1.211
4.5	0.577	0.567	0.567	0.586	0.733	0.727
5	0.784	0.787	0.787	0.819	1.020	1.011
5.5	0.556	0.544	0.544	0.559	0.598	0.609
6	0.755	0.757	0.757	0.779	0.831	0.846
6.5	0.537	0.524	0.524	0.525	0.555	0.564
7	0.730	0.730	0.730	0.734	0.772	0.785
7.5	0.520	0.508	0.508	0.499	0.522	0.528
8	0.707	0.707	0.707	0.699	0.728	0.737
8.5	0.504	0.492	0.492	0.476	0.496	0.502

Stage	Flow Coefficient (Φ)					
	Case 1	Case 2	Case 2S	Case 3	Case 4	Case 5
1	0.521	0.521	0.521	0.521	0.521	0.521
1.5	0.521	0.529	0.511	0.613	0.613	0.613
2	0.521	0.536	0.509	0.645	0.645	0.645
2.5	0.521	0.533	0.495	0.738	0.738	0.738
3	0.521	0.548	0.501	0.794	0.794	0.794
3.5	0.521	0.534	0.483	0.703	0.875	0.703
4	0.521	0.551	0.492	0.768	0.962	0.891
4.5	0.521	0.535	0.475	0.574	0.698	0.722
5	0.521	0.555	0.486	0.585	0.745	0.759
5.5	0.521	0.536	0.467	0.553	0.608	0.627
6	0.521	0.556	0.478	0.570	0.629	0.647
6.5	0.521	0.536	0.460	0.531	0.574	0.588
7	0.521	0.556	0.472	0.546	0.591	0.606
7.5	0.521	0.536	0.455	0.516	0.549	0.559
8	0.521	0.556	0.466	0.531	0.566	0.577
8.5	0.521	0.536	0.449	0.504	0.533	0.541

Table A2 Detailed stage-stacking data (work, flow, shape factor) for all cases

Stage	Stage Pressure Ratio					
	Case 1	Case 2	Case 2S	Case 3	Case 4	Case 5
1	1.398	1.368	1.438	1.077	1.077	1.077
2	1.355	1.345	1.392	1.112	1.112	1.112
3	1.318	1.320	1.350	1.655	1.112	1.655
4	1.288	1.287	1.309	1.622	1.951	1.287
5	1.263	1.263	1.282	1.308	1.479	1.460
6	1.242	1.242	1.258	1.291	1.314	1.321
7	1.223	1.223	1.237	1.257	1.275	1.283
8	1.208	1.206	1.218	1.235	1.244	1.248

Stage	Rotor Work Coefficient					
	Case 1	Case 2	Case 2S	Case 3	Case 4	Case 5
1	0.737	0.718	0.761	0.514	0.514	0.514
2	0.737	0.747	0.766	0.612	0.612	0.612
3	0.737	0.768	0.761	1.119	0.753	1.119
4	0.737	0.764	0.748	1.239	1.577	1.162
5	0.737	0.766	0.749	0.778	1.086	1.041
6	0.737	0.767	0.743	0.803	0.846	0.854
7	0.737	0.764	0.740	0.778	0.814	0.827
8	0.737	0.764	0.737	0.769	0.789	0.795

Stage	Stage Isentropic Power (KW)					
	Case 1	Case 2	Case 2S	Case 3	Case 4	Case 5
1	-821.0	-766.4	-826.8	-567.9	-567.9	-567.9
2	-821.0	-797.3	-832.3	-677.3	-677.3	-677.3
3	-821.0	-818.9	-827.6	-1237.4	-832.5	-1237.4
4	-821.0	-815.4	-813.3	-1370.2	-1760.7	-1297.2
5	-821.0	-817.2	-813.9	-860.7	-1213.0	-1161.8
6	-821.0	-818.7	-807.1	-888.5	-944.1	-953.8
7	-821.0	-815.1	-804.1	-860.1	-908.6	-923.1
8	-821.0	-814.8	-800.9	-850.0	-880.8	-887.6

Stage	Degree of Reaction					
	Case 1	Case 2	Case 2S	Case 3	Case 4	Case 5
1	0.816	0.820	0.810	0.872	0.872	0.872
2	0.816	0.823	0.796	0.999	0.999	0.999
3	0.816	0.817	0.781	1.018	1.146	1.018
4	0.816	0.810	0.770	0.870	1.056	0.926
5	0.816	0.807	0.762	0.798	0.871	0.857
6	0.816	0.804	0.756	0.795	0.817	0.821
7	0.816	0.803	0.752	0.786	0.805	0.810
8	0.816	0.803	0.748	0.779	0.796	0.800

Stage	de Haller Number					
	Case 1	Case 2	Case 2S	Case 3	Case 4	Case 5
1	0.726	0.737	0.712	0.854	0.854	0.854
2	0.726	0.726	0.703	0.850	0.850	0.850
3	0.726	0.716	0.698	0.671	0.835	0.671
4	0.726	0.716	0.699	0.573	0.558	0.640
5	0.726	0.715	0.695	0.710	0.628	0.642
6	0.726	0.713	0.694	0.694	0.692	0.693
7	0.726	0.714	0.693	0.699	0.697	0.695
8	0.726	0.714	0.692	0.699	0.701	0.702

Stage	Shape Factor					
	Case 1	Case 2	Case 2S	Case 3	Case 4	Case 5
1	N.A.	N.A.	N.A.	N.A.	N.A.	N.A.
2	N.A.	*	*	-0.463	*	*
3	N.A.	0.000	0.078	0.019	-0.490	0.488
4	N.A.	0.717	0.104	0.000	0.000	0.000
5	N.A.	0.642	0.326	*	*	0.079
6	N.A.	0.524	0.448	*	*	0.752
7	N.A.	0.951	0.554	0.598	*	0.414
8	N.A.	0.951	*	*	*	0.304

* Out of range

Table A3 Rotor-stator camber line geometries and stage information. Incidence angle i is for the i-th rotor stage and deviation angle δ is for the flow leaving i+0.5th stator.

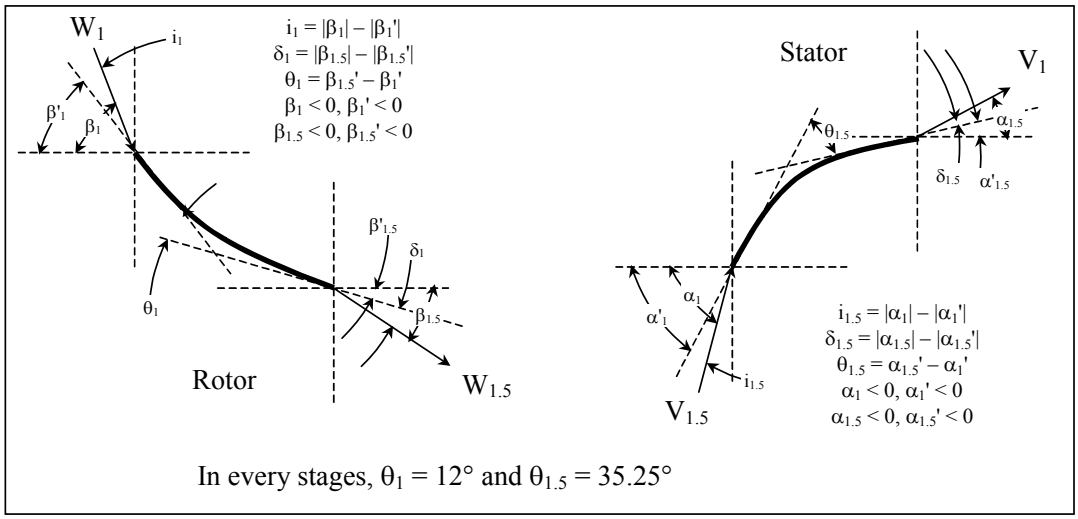

Stage	Hub to Tip Ratio	Tip Diameter (m)	Hub Diameter (m)	$ß_1' / ß_{1.5}'$	$α_1' / α_{1.5}'$	Case 1		Case 2		Case 2S		Case 3		Case 4		Case 5	
						$i_1 / δ_1$	$i_{1.5} / δ_{1.5}$	$i_1 / δ_1$	$i_{1.5} / δ_{1.5}$	$i_1 / δ_1$	$i_{1.5} / δ_{1.5}$	$i_1 / δ_1$	$i_{1.5} / δ_{1.5}$	$i_1 / δ_1$	$i_{1.5} / δ_{1.5}$	$i_1 / δ_1$	$i_{1.5} / δ_{1.5}$
1	0.6357	0.5600	0.3560	-62.47	0.00	0.00	0.00	0.00	0.00	0.00	0.00	0.00	0.00	0.00	0.00	0.00	0.00
1.5	0.6906	0.5418	0.3742	-50.47	35.25	0.00	0.00	0.00	-1.07	0.00	1.41	0.00	-12.53	0.00	-12.53	0.00	-12.53
2	0.7037	0.5376	0.3784	-62.47	0.00	0.00	0.00	0.42	-1.07	-0.27	1.41	1.97	-12.53	1.97	-12.53	1.97	-12.53
2.5	0.7442	0.5252	0.3908	-50.47	35.25	0.00	0.00	0.42	-0.94	-0.27	3.39	1.97	-22.55	1.97	-22.55	1.97	-22.55
3	0.7573	0.5212	0.3948	-62.47	0.00	0.00	0.00	0.96	-0.94	-0.22	3.39	3.80	-22.55	3.80	-22.55	3.80	-22.55
3.5	0.7857	0.5130	0.4030	-50.47	35.25	0.00	0.00	0.96	-0.17	-0.22	5.10	3.80	-15.30	3.80	-30.55	3.80	-15.30
4	0.7977	0.5095	0.4065	-62.47	0.00	0.00	0.00	1.30	-0.17	-0.30	5.10	5.02	-15.30	5.34	-30.55	8.28	-15.30
4.5	0.8181	0.5038	0.4122	-50.47	35.25	0.00	0.00	1.30	0.16	-0.30	6.06	5.02	0.75	5.34	-12.03	8.28	-9.65
5	0.8286	0.5009	0.4151	-62.47	0.00	0.00	0.00	1.53	0.16	-0.39	6.06	2.99	0.75	5.30	-12.03	6.41	-9.65
5.5	0.8441	0.4967	0.4193	-50.47	35.25	0.00	0.00	1.53	0.40	-0.39	7.08	2.99	0.41	5.30	-2.72	6.41	-3.17
6	0.8531	0.4943	0.4217	-62.47	0.00	0.00	0.00	1.65	0.40	-0.59	7.08	2.25	0.41	3.87	-2.72	4.48	-3.17
6.5	0.8651	0.4911	0.4249	-50.47	35.25	0.00	0.00	1.65	0.63	-0.59	7.81	2.25	2.15	3.87	-0.86	4.48	-1.60
7	0.8728	0.4891	0.4269	-62.47	0.00	0.00	0.00	1.70	0.64	-0.77	7.81	1.62	2.15	2.85	-0.86	3.28	-1.60
7.5	0.8822	0.4867	0.4293	-50.47	35.25	0.00	0.00	1.70	0.66	-0.77	8.43	1.62	3.17	2.85	0.69	3.28	0.10
8	0.8888	0.4850	0.4310	-62.47	0.00	0.00	0.00	1.71	0.66	-0.97	8.43	1.16	3.17	2.17	0.69	2.46	0.10
8.5	0.8963	0.4830	0.4330	-50.47	35.25	0.00	0.00	1.71	0.65	-0.97	8.94	1.16	4.12	2.17	1.70	2.46	1.10